

## Distinct Modes of Functional Connectivity induced by Movie-Watching

Murat Demirtaş<sup>1,2</sup>, Adrian Ponce-Alvarez<sup>2</sup>, Matthieu Gilson<sup>2</sup>, Patric Hagmann<sup>4</sup>, Dante Mantini<sup>5,6</sup>,  
Viviana Betti<sup>7</sup>, Gian Luca Romani<sup>8</sup>, Karl Friston<sup>9</sup>, Maurizio Corbetta<sup>10,11</sup>, Gustavo Deco<sup>2,3,12,13</sup>

<sup>1</sup>N3 Division, Department of Psychiatry, Yale University, 40 Temple Street, New Haven, 06511, Connecticut, United States

<sup>2</sup>Center for Brain and Cognition, Computational Neuroscience Group, Department of Information and Communication Technologies, Universitat Pompeu Fabra, Roc Boronat 138, Barcelona, 08018, Spain

<sup>3</sup>Institució Catalana de la Recerca i Estudis Avançats (ICREA), Universitat Pompeu Fabra, Passeig Lluís Companys 23, Barcelona, 08010, Spain

<sup>4</sup>Department of Radiology, Lausanne University Hospital and University of Lausanne (CHUV-UNIL), Rue du Bugnon 46, 1011 Lausanne, Switzerland.

<sup>5</sup>Research Center for Motor Control and Neuroplasticity, KU Leuven, Tervuursevest 101, 3001 Leuven, Belgium.

<sup>6</sup>Functional Neuroimaging Laboratory, IRCCS San Camillo Hospital Foundation, via Alberoni 70, 30126 Venice Lido, Italy.

<sup>7</sup>Department of Psychology, Sapienza University of Rome, via dei Marsi 78, 00185 Rome; Fondazione Santa Lucia and Istituto Di Ricovero e Cura a Carattere Scientifico, 00142, Rome, Italy.

<sup>8</sup>Institute for Advanced Biomedical Technologies, "G. d'Annunzio" University of Chieti-Pescara, 66100, Chieti, Italy.

<sup>9</sup>Wellcome Trust Centre for Neuroimaging, Institute of Neurology, University College London, 12 Queen Square, London WC1N 3BG, United Kingdom.

<sup>10</sup>Department of Neuroscience and Padova Neuroscience Center (PNC), University of Padova, Italy

<sup>11</sup>Departments of Neurology, Radiology, Anatomy of Neurobiology, School of Medicine, Washington University, St. Louis, St Louis, USA

<sup>12</sup>Department of Neuropsychology, Max Planck Institute for Human Cognitive and Brain Sciences, 04103 Leipzig, Germany

<sup>13</sup>School of Psychological Sciences, Monash University, Melbourne, Clayton VIC 3800, Australia

### Corresponding author:

Murat Demirtaş, Yale University, 40 Temple Street, New Haven, 06511, Connecticut, United States.  
[murat.demirtas@yale.edu](mailto:murat.demirtas@yale.edu)

### Funding

GD is supported by the Spanish Research Project PSI2016-75688-P (AEI/FEDER) and by the European Union's Horizon 2020 Framework Programme for Research and Innovation under the Specific Grant Agreement. No. 785907 (Human Brain Project SGA2). MC is supported by NIH grant 5R01NS095741

### Acknowledgements

We thank Alan Anticevic, John Murray, Markus Helmer and Joshua Burt for the insightful discussions and their comments during the preparation of this paper.

1 **Abstract**

2 A fundamental question in systems neuroscience is how endogenous neuronal activity self-  
3 organizes during particular brain states. Recent neuroimaging studies have demonstrated  
4 systematic relationships between resting-state and task-induced functional connectivity (FC).  
5 In particular, continuous task studies, such as movie watching, speak to alterations in  
6 coupling among cortical regions and enhanced fluctuations in FC compared to the resting-  
7 state. This suggests that FC may reflect systematic and large-scale reorganization of  
8 functionally integrated responses while subjects are watching movies. In this study, we  
9 characterized fluctuations in FC during resting-state and movie-watching conditions. We  
10 found that the FC patterns induced systematically by movie-watching can be explained with a  
11 single principal component. These condition-specific FC fluctuations overlapped with inter-  
12 subject synchronization patterns in occipital and temporal brain regions. However, unlike  
13 inter-subject synchronization, condition-specific FC patterns were characterised by increased  
14 correlations within frontal brain regions and reduced correlations between frontal-parietal  
15 brain regions. We investigated these condition-specific functional variations as a shorter time  
16 scale, using time-resolved FC. The time-resolved FC showed condition-specificity over time;  
17 notably when subjects watched both the same and different movies. To explain self-  
18 organisation of global FC through the alterations in local dynamics, we used a large-scale  
19 computational model. We found that condition-specific reorganization of FC could be  
20 explained by local changes that engendered changes in FC among higher-order association  
21 regions, mainly in frontal and parietal cortices.

## 22 **Introduction**

23 The neural correlates of information processing at a local scale have been widely studied.  
24 However, the integration of information at the whole-brain level may also be crucial for  
25 understanding brain function (Baars, 1993; Tononi, 2004). Advances in neuroimaging  
26 techniques such as functional magnetic resonance imaging (fMRI) now allow us to ask how  
27 the brain regulates information flow in large-scale cortical networks (Deco et al., 2015). For  
28 example, several studies suggest that neuronal synchronization mediates communication in  
29 large-scale cortical networks during task performance (Brovelli et al., 2004; Gross et al.,  
30 2004; Siegel et al., 2008) and the resting state (Brookes et al., 2011; Hipp et al., 2012).

31

32 Resting state functional connectivity (rs-FC) is a widely-used technique to characterize large-  
33 scale organization of brain activity, based on the temporal correlations between blood oxygen  
34 level-dependent (BOLD) signals (Biswal et al., 1995). Rs-FC patterns have been shown to  
35 provide ‘fingerprints’ for functional brain organization during the resting-state (Finn et al.,  
36 2015; Smith, 2016) and task induced responses (Tavor et al., 2016). Recent studies suggest  
37 a strong relationship between the FC during resting state and task performance (Betti et al.,  
38 2013; Cole et al., 2016, 2014; Rosenberg et al., 2015). In particular, continuous task  
39 paradigms such as viewing natural scenes (i.e. movie watching) are of particular interest due  
40 to their ecological validity (Betti et al., 2013). Several studies have found that FC is more  
41 reliable and promotes the detection of individual differences while subjects view movies (Kim  
42 et al., 2017; Vanderwal et al., 2017, 2015). Moreover, a systematic reorganization of the  
43 cortical interactions – with changes in functional network assignments – has been  
44 demonstrated during movie-watching (Kim et al., 2017; Wolf et al., 2010). Therefore, the  
45 condition-specific changes and enhanced reliability of FC may be induced by the task-  
46 dependent engagement of specific brain regions (Hasson, 2004; Hasson et al., 2010) and/or  
47 large-scale functional reorganization (Kim et al., 2017; Simony et al., 2016; Wolf et al., 2010).  
48 On the basis of these studies, we hypothesized that the intrinsic reorganization of FC during  
49 movie-watching could be quantified and modelled in terms of systematic fluctuations in  
50 connectivity patterns.

51

52 To study the reorganization of FC, we analysed the variations in grand-average (over time)  
53 and time-resolved FC during rest and movie-watching. We characterized the variations in FC  
54 patterns across subjects using principal component analysis (PCA). PCA and associated  
55 techniques have been used to characterize resting-state fluctuations (Carbonell et al., 2011),  
56 whole-brain connectivity dynamics (Allen et al., 2012) and disease-related rs-FC states  
57 (Craddock et al., 2009). Based on the projections of individual subject scores on the principal  
58 components, we identified FC-states specific to the movie-watching condition. We then  
59 compared these condition-specific FC patterns with inter-subject synchronization (Kim et al.,  
60 2017; Simony et al., 2016).

61

62 One question – related to the task-dependent reorganization of FC – is whether alterations in  
63 grand-average FC (over the whole session) reflect a continuous (temporally stable) functional  
64 state or the emergence of functional modes fluctuating over time (Gonzalez-Castillo et al.,  
65 2015). To answer this question, we extended our analysis beyond grand-average FC states  
66 and investigated the temporal fluctuations in FC states based on the dynamics of phase-  
67 coupling among brain regions.

68

69 Finally, we used whole-brain computational modelling to test whether the reorganization of  
70 FC can be explained by the fluctuations in local connectivity. In other words, we adopted a  
71 mechanistic approach to task-dependent FC using a large-scale, biophysically plausible  
72 modelling framework. In brief, we constrained long-range interactions between brain regions  
73 using diffusion weight imaging-derived (DWI) structural connectivity, and estimated the  
74 fluctuations in local connectivity – of each brain region – during movie-watching that best  
75 explained the observed FC.

76

77 **Results**

78 To characterize fluctuations in functional connectivity (FC), first we established the  
79 relationship between the FC patterns during resting-state and movie-watching conditions. The  
80 grand average FC over the resting-state and movie-watching sessions exhibited similar  
81 patterns ( $r=0.8$ ) (**Figure 1A**). The similarity among the FC of individual subjects was  
82 substantially higher under the same condition (*resting-state*  $r=0.46 \pm 0.06$ ; *movie*  $r=0.49 \pm$   
83  $0.06$ ) than across conditions ( $r=0.40 \pm 0.07$ ). These results confirm previous findings that  
84 showed similar grand average FC patterns during resting-state and movie-watching (Betti et  
85 al., 2013; Cole et al., 2014).

86  
87 To quantify the variability in FC across subjects during resting-state and movie-watching  
88 conditions, we performed principal component analysis (PCA) over subjects (**Figure 1B**).  
89 PCA decomposes high-dimensional data features into orthogonal axes (principal  
90 components) that explain the most variance. The projections provide a score for each  
91 observation (i.e., subject/run) along the principal components. We applied PCA to  
92 concatenated vectorised matrices from 21 subjects, during 2 separate runs of resting state  
93 and movie-watching conditions. This allows us to compare the scores (i.e. expression of  
94 principal components by individual subjects) during rest and movie-watching.

95

96 **Distinct modes of variation in functional connectivity during movie-watching**

97

98 The first principal component (PC-1) – explaining 25.8% of the variance (**Figure 1C**) –  
99 reflected a FC pattern that was conserved over runs. The scores of PC-1 were significantly  
100 correlated with the global variance of each fMRI run ( $r=0.99$ ,  $p<0.0001$ ,  $dof=83$ ) (**Figure 1L**).  
101 This result suggests that the principal mode of variation in FC reflects variations in global  
102 signal. The second principal component (PC-2) (**Figure 1E**) – explaining 7.2% of the variance  
103 – clearly distinguished the movie-watching condition from resting-state (i.e., PC-2 scores  
104 perfectly separate resting-state and movie-watching conditions). We will refer to this  
105 component as a condition-specific PC (**Figure 1F**). This result suggests that the condition-  
106 specific variations in FC can be explained along a single mode of variation (PC-2), which is  
107 orthogonal to the global-signal related mode (PC-1).

108

109 We repeated PCA for 1000 surrogate FCs across subjects to define the components  
110 explaining a significant proportion of variance (**see Materials and Methods**). The variance  
111 explained by the first 13 components was greater than the variance explained by surrogate  
112 FCs; suggesting that the first 2 PCs explain a significant amount of variation. The remaining  
113 components did not show any specificity regarding the movie-watching condition and were  
114 not analysed further.

115

116 To test the consistency of the condition-specific PCs across runs, we repeated the PCA for  
117 each run separately and quantified the similarities between PCs across runs. For each run,  
118 we identified condition-specific PCs that were highly consistent across runs ( $r=0.83$  for PC-2  
119 scores) (**Supplementary Figure 1**). Furthermore, the similarities between PCs and scores  
120 were higher for condition-specific components than global signal-related components ( $r=0.75$   
121 for PC-1 scores) (**Supplementary Figure 1**). These results suggested that the condition-  
122 specific PC and associated scores (i.e., expression in individual subjects) were conserved  
123 across runs, which suggest a link between condition-specific and individual variations in FC.

124

### 125 **Contribution of potential non-neuronal confounds**

126

127 Previous studies have shown differential subject movements and increased arousal while  
128 watching natural scenes (Siegel et al., 2016; Vanderwal et al., 2015). Therefore, the  
129 condition-specific PC may reflect the contributions from movement or arousal artefacts. To  
130 address the role of head motion, we calculated the correlation between mean frame-wise  
131 displacement and principal component scores. The first PC scores, reflecting global signal  
132 variations, were significantly correlated with head motion (*Spearman rank*  $r=0.37$ ,  $p<0.001$ ,  
133  $dof=83$ ). We found no significant correlation between head motion and condition-specific PC  
134 scores (*Spearman rank*  $r=0.03$ ,  $p=0.75$ ,  $dof=83$ ).

135

136 To preclude other artefactual contributions, we repeated the analyses after regressing out the  
137 global signal (**Figure 1G-J**). After global signal regression (GSR) the first principal component  
138 (PC-1) explained 9.69% of the variance and reflected condition-specific variations in FC  
139 (**Figure 1J**). Similarly, no significant correlation was observed between head motion and  
140 condition-specific PC scores after GSR (*Spearman rank*  $r=0.02$ ,  $p=0.85$ ,  $dof=83$ ). Crucially,  
141 the condition-specific components were similar with and without GSR ( $r=0.81$ ) (**Figure 1K**).  
142 This analysis suggests that condition-specific variations in FC are not associated with head  
143 motion and that they are robust to global signal regression.

144

### 145 **Relationship between condition-specific FC variations and inter-subject** 146 **synchronization**

147

148 The condition-specific variations in FC may reflect time-locked fluctuations during movie-  
149 watching condition as reported in previous studies (Kim et al., 2017; Simony et al., 2016). We  
150 characterized these time-locked FC patterns (during the movie-watching condition) using  
151 inter-subject synchronization FC (ISS-FC) (**Figure 2A**). In brief, ISS-FC removes the  
152 contribution of endogenous activity by evaluating the FC between two regions from different  
153 subjects (Kim et al., 2017; Simony et al., 2016). For each run, the subjects were randomly  
154 assigned into 2 non-overlapping groups. The FC was then evaluated as the correlation  
155 between pairs of regions across the average BOLD time-series from distinct sets of subjects.

156 Since the subjects were exposed to the same stimuli only during movie watching, ISS-FC  
157 exhibited high-magnitude correlations in the movie-watching but not in the resting-state  
158 condition (Kim et al., 2017) (**Supplementary Figure 2**).

159  
160 ISS-FC during movie watching showed the highest values within occipital and temporal  
161 regions; suggesting that synchronization is due to time-locked visual and auditory events  
162 (**Figure 2B**). In addition, ISS-FC showed high synchronization between occipital/temporal and  
163 parietal brain regions, such as inferior and superior parietal cortex (**Figure 2B**). The pattern of  
164 the condition-specific PC was similar to the ISS-FC ( $r=0.46$ ) (**Figure 2C-D**). As in the ISS-FC,  
165 the condition-specific PC exhibited higher values within occipital and temporal, and between  
166 occipital/temporal and parietal brain regions (**Figure 2C**). However, the condition-specific PC  
167 differed from the ISS-FC in various aspects: First, the condition-specific PC exhibited more  
168 pronounced connectivity changes in fusiform and lingual gyri, and inferior temporal compared  
169 to the ISS-FC. Second, the condition-specific PC comprised enhanced intra- and inter-  
170 hemispheric connectivity between frontal brain regions (particularly lateral and medial orbital  
171 frontal cortex, pars orbitalis and frontal pole), which were not observed in the ISS-FC. Third,  
172 the condition-specific PC exhibited strong negative values (reduced connectivity) particularly  
173 across frontal and parietal regions. These attenuated values involved FC between caudal  
174 anterior/posterior cingulate and supramarginal gyrus, superior/inferior parietal, and caudal  
175 middle-frontal cortex. These results suggest that although the condition-specific PC overlaps  
176 with the ISS-FC, it highlights a distinct functional reorganization, expressed predominantly in  
177 higher-order association regions.

178

### 179 **Condition-specific FC trajectories in time-resolved FC**

180

181 The grand average FC approach cannot **differentiate** between a temporally stable mode of  
182 FC and fluctuations in FC (i.e., a succession of distinct FC patterns). To address this issue,  
183 we analysed time-resolved fluctuations in FC (also known as dynamic FC). Here, we tested  
184 the hypothesis that FC continuously reorganizes during movie-watching. We constructed  
185 time-resolved FC based on the fluctuations in phase-locking values (PLVs) between brain  
186 regions (see **Materials and Methods**). The advantage of this approach is that it eliminates  
187 the dependency on a particular window and step size, as in sliding-window analysis. Instead,  
188 it requires one to specify a narrowband range to calculate PLVs. Here, we chose *0.04-*  
189 *0.07Hz*, which does not overlap with the frequency ranges of low-frequency drift and high-  
190 frequency noise (Glerean et al., 2012). First, we band-pass filtered the BOLD time-series and  
191 employed Hilbert transform. We then calculated the PLVs at each time point using the  
192 instantaneous phases of each brain region (**Figure 3A**).

193

194 To establish the link between the time-resolved FC analyses and Pearson correlation-derived  
195 FC, we calculated the grand average PLVs over time, and performed PCA **across** subjects.

196 This analysis showed that the principal components based on PLVs also exhibit condition  
197 specificity (**Figure 3D**). Furthermore, condition-specific PC of PLVs was similar to those  
198 derived from Pearson correlation-derived FC ( $r=0.88$ ). Therefore, the condition specific FC  
199 patterns for PLVs were aligned with those based on the Pearson correlation-derived grand-  
200 average FC.

201

202 For each subject, we performed PCA on PLVs over time (**Figure 3B**). We identified the  
203 condition-specific component for each subject as the one (i.e. PC-1 or PC-2) exhibiting the  
204 highest correlation with the grand-average condition-specific component (**Figure 3E**). For the  
205 majority of the subjects, the trajectories (i.e. the PC scores) of the condition-specific  
206 components reflected a clear distinction between conditions (**Supplementary Figure 3**). We  
207 quantified this condition-specificity for each individual subject by comparing the median  
208 trajectories (i.e. median PC scores) during the resting-state and the movie-watching  
209 conditions (**Figure 3C**). We then calculated the distance (i.e. squared difference) between the  
210 median trajectories of rest/movie conditions (**Figure 3F**). The distance between rest/movie  
211 median trajectories were compared to the distance between 1000 randomly grouped  
212 trajectories (**Figure 3G**). 20 out of 21 subjects showed a significantly larger distance between  
213 rest/movie trajectories than any other randomly grouped trajectories ( $p<0.001$ ) (**Figure 3I**).  
214 Since the trajectories of the condition-specific PCs are time-dependent, we assessed the  
215 significance of the median trajectory distances between runs/conditions across subjects. We  
216 found that the distance across conditions (i.e. movie/rest conditions) were significantly larger  
217 than the distance across runs (i.e. rest/rest and movie/movie runs) ( $p<0.0001$ , *permutation t-*  
218 *test, 10000 permutations*) (**Figure 3H**). We found no significant difference between the  
219 distance across runs for resting state and movie conditions ( $p=0.82$ , *permutation t-test, 10000*  
220 *permutations*) (**Figure 3H**). These results speak to the emergence of a conserved FC pattern  
221 during movie-watching condition on a short timescale.

222

### 223 **Condition-specific FC patterns within and across runs**

224

225 To study the role of time-locked events on PLV dynamics during movie-watching (analogous  
226 to inter-subject synchronization), we calculated the similarity between instantaneous PLVs  
227 across conditions and runs. In brief, for each time point, we calculated the similarity between  
228 the PLVs of a single subject ( $k$ ) and the average PLVs across the rest of the subjects ( $n\neq k$ ).  
229 The average PLVs were calculated to test the PLV similarity in 3 different cases: Across  
230 conditions (e.g. if subject  $k$  is at resting state run 1, the average PLVs were calculated for  
231 movie-watching run 1), across runs (e.g. if subject  $k$  is at resting state run 1, the average  
232 PLVs were calculated for resting state run 2) and within runs (e.g. if subject  $k$  is at resting  
233 state run 1, the average PLVs were calculated for resting state run 1) (**Figure 4A**).

234

235 Both for resting-state and movie-watching conditions, the similarity across runs was  
236 significantly higher than the similarity across conditions ( $p < 0.0001$  for both runs: permutation  
237 *t*-test, 10000 permutations) (**Figure 4B-E**), confirming the continuous functional  
238 reorganization during movie-watching condition. Furthermore, this result shows that during  
239 movie-watching, the similarity between instantaneous PLVs was higher, even when the  
240 subjects were viewing different scenes. For resting state runs, the average similarity between  
241 instantaneous PLVs did not show any significant difference across runs ( $p = 0.54$  for run 1,  
242  $p = 0.34$  for run 2, permutation *t*-test, 10000 permutations) (**Figure 4B, C**). In contrast, the  
243 average similarity between instantaneous phase-locking was significantly higher for the same  
244 movie runs than across runs ( $p < 0.0001$  for both runs: permutation *t*-test, 10000 permutations,  
245  $p < 0.0001$ ) (**Figure 4D,E**). These results indicate that the PLV dynamics during movie-  
246 watching reflects both the effects of time-locked events and a continuous functional  
247 reorganization.

248

#### 249 **Large-scale computational modelling of the regional dynamics underlying movie-** 250 **watching FC**

251

252 Both the grand average and time-resolved FC analyses suggested a functional reorganization  
253 during movie-watching. Based on these results, we hypothesized that the variations in  
254 regional dynamics could explain the functional reorganization. We used a Hopf normal model  
255 to characterize the BOLD activity of each region (Deco et al., 2017). The regions were  
256 coupled to each other via DWI-derived structural connectivity scaled by a global coupling  
257 parameter (**Figure 5A**). The dynamics of each region were governed by a local bifurcation  
258 parameter ( $a$ ). The local bifurcation parameters ( $a$ ) reflect whether an individual region is in a  
259 noise-driven regime ( $a < 0$ ), oscillatory regime ( $a > 0$ ), or alternates between the two regimes  
260 ( $a \sim 0$ ) (**Figure 5A**). We estimated the global coupling and local bifurcation parameters of  
261 each subject/run by maximizing the similarity (i.e. Pearson correlation) between empirical and  
262 model FCs using gradient-descent. We found no significant difference between the model fits  
263 for resting-state ( $r = 0.518 \pm 0.057$ ) and movie-watching conditions ( $r = 0.497 \pm 0.045$ ) ( $p = 0.146$ ,  
264 permutation *t*-test, 10000 permutations). To characterize the overall topography underlying  
265 each condition, first we estimated the optimal global coupling parameter ( $g$ ) and optimal  
266 bifurcation parameters ( $a$ ) for resting state and movie watching condition. At rest, the average  
267 bifurcation parameter estimates were low in parietal and temporal regions, whereas they were  
268 higher in occipital and frontal regions (**Figure 5B**). For movie condition, the bifurcation  
269 parameters were elevated in parietal and temporal regions and decreased in anterior  
270 cingulate, lateral prefrontal cortices and in supramarginal gyrus (**Figure 5C**). There was no  
271 difference between the mean optimal bifurcation parameters of rest and movie conditions  
272 (**Figure 5D**).

273

274 To quantify the difference between conditions, we compared the optimal global coupling and  
275 bifurcation parameters of the resting-state and the movie-watching conditions (**Figure 6A**).  
276 We found no significant difference in global coupling parameters between rest and movie  
277 conditions ( $p=0.719$ , permutation *t*-test, 10000 permutations) (**Figure 6B**). In the movie  
278 condition, the local bifurcation parameters were significantly decreased – towards negative  
279 values – in bilateral caudal anterior cingulate, right supramarginal gyrus, and left postcentral  
280 cortex (**Figure 6D**). In contrast, the bifurcation parameters were significantly increased in  
281 bilateral orbital frontal and lateral orbital frontal cortices, left medial temporal cortex, right  
282 frontal pole, middle rostral frontal and superior parietal cortex cortices (**Figure 6D**). These  
283 changes in higher-order association regions are consistent with the patterns observed in  
284 condition-specific PC.

285

286 Finally, we repeated the PCA on the bifurcation parameter estimates across subjects and  
287 conditions (**Figure 6E-G**). The scores of the first principal component (PC-1) – explaining  
288 41.77% of variance – and the second principal component (PC-2) – explaining 10.25% of  
289 variance – were both significantly correlated with the scores of the empirically observed  
290 condition-specific PC (*PC-1 Spearman rank*  $r=0.44$ ,  $p=0.004$ ,  $dof=41$ ; *PC-2 Spearman rank*  
291  $r=0.63$ ,  $p<0.0001$ ,  $dof=41$ ; *PC-1+PC-2 Spearman rank*  $r=0.73$ ,  $p<0.0001$ ,  $dof=41$ ). The first  
292 principal component (PC-1) exhibited a strong positive peak in precuneus and isthmus of  
293 cingulate; with slightly higher values in medial frontal and temporal regions, which is very  
294 similar to default mode network (DMN) topography (**Figure 6E**). The second principal  
295 component (PC-2) had higher values in temporal and frontal regions as observed in the  
296 contrast between conditions (**Figure 6F**). Furthermore, the scores of the first and second  
297 principal components were negatively correlated in, and only in, the movie-watching condition  
298 (*Spearman rank*  $r=-0.496$ ,  $p=0.02$ ,  $dof=20$ ) (**Figure 6G**). These results suggest that the  
299 changes in local connectivity during the movie-condition engender multiple modes of  
300 variation, which reflect condition-specific and DMN-like topographies.

301 **Discussion**

302 In this paper, we investigated the reorganization of functional connectivity (FC) during movie-  
303 watching condition. We showed that during movie-watching FC patterns vary along a single  
304 mode of variation (i.e. a condition-specific pattern of connectivity that captures the variations  
305 across subjects), which emerges as a continuous functional state over time.

306

307 We used principal component analysis (PCA) to characterize the variations in FC across  
308 individuals and conditions (i.e. resting-state vs. movie-watching). We found that the principal  
309 component (PC-1) reflected the variations in global signal, whereas the second principal  
310 component (PC-2) reflected the distinction between resting-state and movie-watching  
311 conditions. We investigated the patterns of the condition-specific component in the context of  
312 inter-subject synchronization FC (ISS-FC) (Kim et al., 2017; Simony et al., 2016). The  
313 connectivity patterns of the condition-specific component were similar to the ISS-FC. Both  
314 characterizations of FC highlighted intra- and inter-hemispheric connectivity within occipital  
315 and temporal regions as well as their connections with parietal regions. These results **are**  
316 **consistent with increased intra- and inter-network connectivity in auditory/language**  
317 **networks (Betti et al., 2013; Vanderwal et al., 2015) and visual network (Vanderwal et**  
318 **al., 2015) during movie watching. Our results** suggest that the enhanced communication  
319 between regions related to audiovisual processing and attention are primarily driven by the  
320 time-locked events during movie-watching (Hasson, 2004; Hasson et al., 2010). **This**  
321 **interpretation may explain the larger grouping of visual, auditory and attention**  
322 **networks during the processing of scenes (Kim et al., 2017).**

323

324 However, unlike ISS-FC, condition-specific fluctuations showed enhanced connectivity within  
325 frontal brain regions and reduced connectivity between frontal-parietal brain regions and  
326 cingulate (e.g. supramarginal gyrus, superior/inferior parietal cortex, caudal middle frontal  
327 cortex vs. anterior and posterior cingulate cortex). These results are consistent with previous  
328 studies of functional reorganization during movie-watching (Kim et al., 2017; Simony et al.,  
329 2016; Wolf et al., 2010). **Furthermore, the frontal-parietal network has been shown to**  
330 **exhibit higher inter-individual variability during movie watching (Vanderwal et al., 2017,**  
331 **2015). Our results also support the relationship between individual- and condition-**  
332 **specific FC variations in fronto-parietal regions.** We argue that – during movie-watching –  
333 reorganization of FC with the primary sensory regions is mainly driven by extrinsic factors  
334 such as sensory stimulation, whereas the higher-order association regions exhibit a self-  
335 organisation of endogenous activity.

336

337 The existence of a condition-specific component in grand-average FC may not be sufficient to  
338 draw conclusions about the functional reorganization during movie-watching. Therefore, we  
339 asked how the condition-specific PC topography relates to the time-resolved FC. We used the  
340 Hilbert transform of narrowband filtered BOLD time-series, and characterized time-resolved

341 FC based on phase-locking values over time. We found condition-specific components on  
342 grand average PLVs over subjects as well as individual PLVs over time. The trajectories of  
343 the condition-specific PLV components suggested that this component might appear as a  
344 stable state during movie-watching. We substantiated this conclusion by analysing the  
345 similarity between instantaneous PLVs and average PLVs (over subjects), under different  
346 conditions/runs. The similarity was significantly lower when the subjects were scanned under  
347 different conditions (i.e. rest vs. movie) than they were under same condition (i.e. rest vs. rest  
348 and movie vs. movie). Furthermore, only during movie-watching, did we find that PLV  
349 similarity was higher for subjects in the same run (i.e. run 1 vs. run 1) than subjects in the  
350 different runs (i.e. run 1 vs. run 2). Overall, these results suggested that whole-brain FC (in  
351 the time-scale of BOLD signals) is continuously reconfigured on a short time scale. **Previous**  
352 **studies found that the dynamics of ISS-FC states are highly robust, depending on the**  
353 **narrative of a story; although the FC patterns were similar over time (Simony et al.,**  
354 **2016). Our results suggest that the dynamics of condition-specific FC states exhibit**  
355 **both continuous and time-locked components.** We speculate that the functional  
356 reorganization in higher-order association regions may reflect the adaptation of the brain's  
357 intrinsic architecture to mediate large-scale information flow during movie-watching.

358

359 Previous studies have reported decreased head movements and higher arousal while movie-  
360 watching (Siegel et al., 2016; Vanderwal et al., 2015). Therefore, the emergence of a  
361 condition-specific FC component could also reflect systematic artefacts. In this study, we  
362 found no significant differences between mean frame-wise displacements (head motion) of  
363 the subjects across conditions. However, we observed that head motion was significantly  
364 altered while watching movie (i.e. during movie-watching condition some subjects moved  
365 less, whereas others move more). The scores of the condition-specific PC were not  
366 correlated with the mean frame-wise displacements or the PC scores associated with head  
367 motion. However, both measures were significantly correlated with the PC scores reflecting  
368 global signal variations. To rule **out** the possibility of other confounds, we repeated the  
369 analysis and identified similar condition-specific component after performing global signal  
370 regression (GSR), which was replicated across runs. Apart from the head motion and global  
371 signal analyses, the contribution of non-neuronal confounds is unlikely, given the results:  
372 First, the variations in occipital and temporal regions in condition-specific component  
373 substantially overlaps with inter-subject synchronization (no changes were observed in  
374 somatomotor brain regions), which relies on the covariation between brain regions averaged  
375 over different subjects. Although the sensory-motor brain regions are known to be more  
376 susceptible to non-neuronal confounds (Bijsterbosch et al., 2017; Power et al., 2017), these  
377 results are more likely explained by common audiovisual stimulation than synchronization of  
378 head motion or respiration across subjects. Second, the condition-specific components were  
379 very similar across runs, and narrowband filtered data (0.04-0.07Hz). Known artefactual  
380 sources such as low-frequency drift, cardiac and respiratory variations are often associated

381 with lower or higher frequencies (Glerean et al., 2012). Therefore, substantial variations in the  
382 condition-specific component would be expected in the narrow-band signals, if they were  
383 related to these confounding factors.

384

385 Our results suggested a distinct and continuous reorganization of FC during movie-watching.  
386 Under the assumption that structural connectivity does not change, one can use whole-brain  
387 computational modelling to characterize local variations in neurodynamics during movie-  
388 watching. Here, we used Hopf normal model to characterize BOLD signals. The motivation  
389 behind using this model was that noise-driven and oscillatory dynamics can be modelled  
390 using a single parameter (local bifurcation parameter). When the local bifurcation parameter  
391 of a particular region is negative, each region exhibits noise-driven dynamics. For positive  
392 bifurcation parameter values, the region exhibits sustained oscillations. Therefore, higher  
393 parameters values of a region in the model indicate that the region has larger influence on its  
394 connected regions. The model revealed significant decreases in bifurcation parameters  
395 particularly in anterior cingulate cortex and in supramarginal gyrus, which suggested an  
396 association between decreased bifurcation parameters and the key regions that exhibited  
397 suppressed connectivity patterns in the component-specific PC. In contrast, the bifurcation  
398 parameters increased in lateral prefrontal cortex, medial temporal cortex and superior parietal  
399 regions. These results suggest that endogenous activity in higher-order association regions  
400 are altered during movie-watching. Nevertheless, it is important to note that the model  
401 describes the BOLD signals in the associated low-frequency narrow-band. Therefore, the  
402 results should be interpreted only in relation to low-frequency fluctuations in BOLD signals.

403

404 The PCA over model parameters revealed two different modes of variation that were  
405 associated with the FC condition-specific variations. Although the second PC was more  
406 consistent with the alterations in empirical and model data, the first PC also showed  
407 substantial conditional-specificity. Interestingly, the first PC exhibited a pattern typical of  
408 default mode network (DMN), which involves the isthmus cingulate, precuneus, medial frontal  
409 and temporal cortices. Furthermore, the associated PC scores were negatively correlated  
410 across subjects in only the movie-watching condition. Therefore, the model predicts that the  
411 interaction between condition-specific and DMN-like activation patterns has a crucial role in  
412 the reorganization of FC. **This prediction is consistent with the robust and reproducible**  
413 **reconfiguration of DMN during narrative comprehension (Simony et al., 2016).**  
414 **Particularly, we observed that the local bifurcation parameters of the DMN regions**  
415 **shifted towards the critical point (i.e.  $a=0$ ), which may explain the emergence of the**  
416 **robust and reproducible dynamical DMN configurations.** However, based on these  
417 results, it is not possible to draw conclusions on the causal mechanisms that drive the  
418 relationship between DMN and condition-specific networks. The most important caveat is the  
419 lack of individual-specific estimates for structural connectivity. Therefore, the emergence of  
420 DMN-like component may simply reflect an additional mode of variation that compensates for

421 the lack of variability in individual-specific structural connections. However, the results may  
422 also indicate that several regions of DMN (particularly **the** precuneus) **have** a role in  
423 mediating the switch between distinct functional states, which is consistent with previous  
424 studies showing that precuneus dynamically binds to distinct functional networks (Utevsky et  
425 al., 2014). An alternative explanation may involve the variations of arousal and vigilance  
426 levels. This explanation is consistent with a selective neuromodulatory enabling of intrinsic  
427 synaptic connections by ascending modulatory neurotransmitter systems (e.g., noradrenaline)  
428 (Shine et al., 2018). This is particularly relevant in light of the systematic changes in the local  
429 bifurcation parameter that showed regionally-specific and condition-sensitive effects in our  
430 modelling analyses. Recent studies showed the relationship between transcriptomic  
431 variations and task-related alterations (Shine et al., 2018) as well as microcircuit  
432 specialization (Burt et al., in Press) in the human brain. These advances may allow  
433 systematic investigation of the mechanisms behind the functional reorganization of the brain.

434

435 Finally, several limitations should be noted while interpreting the results in this paper. The  
436 most important limitation of this study is the small sample size (21 subjects). Therefore, the  
437 results require replication in an independent dataset. In addition, the design of this study did  
438 not allow us to compare the results with other conditions (such as a different movie). Although  
439 different runs involved different scenes of the same movie, previous studies have found  
440 differences in FC regarding the type/familiarity of the movie (i.e. abstractness, social content)  
441 (Vanderwal et al., 2015; Wolf et al., 2010). Future studies may investigate the variants of the  
442 movie-watching condition, different tasks and/or other continuous experimental paradigms  
443 (e.g. reading, social interactions, etc.). Another important limitation of this study is the use of  
444 coarse (33 regions per hemisphere), anatomically defined parcellation. Recently developed  
445 cortical parcellations offer functional (or multimodal) definitions of cortical areas, which also  
446 facilitate better mapping of functional networks. Our coarse parcellation of **the** cortex had  
447 advantages particularly for time-resolved FC analysis and whole-brain modelling due to  
448 computational efficiency and the implicit reduction in the number of parameters. Techniques  
449 such as independent component analysis may provide better characterization of time-  
450 dependent states. Such analytical extensions would require longer recording sessions and a  
451 better definition of the cortical areas. A limitation regarding the computational modelling is that  
452 the model relies on average DWI-derived SC, which may fail to detect interhemispheric  
453 connections, individual variations, and is insensitive to directed connections. Previous studies  
454 have shown that the changes in directed effective connectivity may also play role in defining  
455 the reorganization of FC (Gilson et al., 2017), which may explain lack of significant  
456 differences in visual cortex. Effective connectivity – as assessed using dynamic causal  
457 modelling studies of the resting state – also point to a modulation of regional excitability by  
458 different components of the default mode. For example, previous studies revealed that the  
459 influence of the SN (salience network) and DAN (dorsal attention network) on the DMN

460 (default mode network) regions is inhibitory; whereas the DMN exerted an excitatory influence  
461 on the SN and DAN regions (Zhou et al., 2018).

462

463 Current experimental paradigms are optimal **for the study of** task-dependent changes in  
464 BOLD signals, but these may not reveal the dynamic organization of whole-brain FC. Unlike  
465 other task-evoked experimental approaches, continuous task paradigms offer a contextual  
466 environment (e.g. movie-watching), which engage a collection of processes (e.g. audiovisual  
467 processing, attention, social cognition...etc.) contextualized by the stimuli. Our findings  
468 suggest that continuous task experiments may be useful to study how humans hierarchically  
469 reorganize its internal representations to adapt to environmental context (Friston, 2010).  
470 Impairments in these adaptation mechanisms may explain the symptoms in various mental  
471 disorders such as schizophrenia (Stephan et al., 2016). Future studies with more  
472 sophisticated continuous experimental designs may reveal richer dynamical manifestation of  
473 functional reorganization such as consolidation of particular functional states in time (i.e.  
474 adaptation) and/or emergence of observable transient functional states (i.e. multistability).

475 **Materials and Methods**

476 **Study design**

477

478 The fMRI imaging data used in this paper have been described in details elsewhere (Betti et  
479 al., 2013; Mantini et al., 2012). Twenty-four right-handed young, healthy volunteers (15  
480 females, 20–31 years old) participated in the study. They were informed about the  
481 experimental procedures, which were approved by the Ethics Committee of the Chieti  
482 University, and signed a written informed consent. The study included a resting state and a  
483 natural vision condition. In the resting state, participants fixated a red target with a diameter of  
484 0.3 visual degrees on a black screen. In the natural-vision condition, subjects watched (and  
485 listened) to 30 minutes of the movie “The Good, the Bad and the Ugly” in a window of  
486 24x10.2 visual degrees. Visual stimuli were projected on a translucent screen using an LCD  
487 projector, and viewed by the participants through a mirror tilted by 45 degrees. Auditory  
488 stimuli were delivered using MR-compatible headphones.

489

490 **Data acquisition**

491

492 Functional imaging was performed with a 3T MR scanner (Achieva; Philips Medical Systems,  
493 Best, The Netherlands) at the Institute for Advanced Biomedical Technologies in Chieti, Italy.  
494 The functional images were obtained using T2\*-weighted echo-planar images (EPI) with  
495 BOLD contrast using SENSE imaging. EPIs comprised of 32 axial slices acquired in  
496 ascending order and covering the entire brain (32 slices, 230 x 230 in-plane matrix,  
497 TR/TE=2000/35, flip angle = 90°, voxel size=2.875x2.875x3.5 mm<sup>3</sup>). For each subject, 2 and  
498 3 scanning runs of 10 minutes duration were acquired for resting state and natural vision,  
499 respectively. Each run included 5 dummy volumes – allowing the MRI signal to reach steady  
500 state, and an additional 300 functional volumes that were used for analysis. Eye position was  
501 monitored during scanning using a pupil-corneal reflection system at 120 Hz (Iscan,  
502 Burlington, MA, USA). A three-dimensional high-resolution T1-weighted image, for anatomical  
503 reference, was acquired using an MP-RAGE sequence (TR/TE=8.1/3.7, voxel  
504 size=0.938x0.938x1 mm<sup>3</sup>) at the end of the scanning session.

505

506 **Data preprocessing**

507

508 Data preprocessing was performed using SPM5 (Wellcome Department of Cognitive  
509 Neurology, London, UK) running under MATLAB (The Mathworks, Natick, MA). The  
510 preprocessing steps involved the following: (1) correction for slice-timing differences (2)  
511 correction of head-motion across functional images, (3) coregistration of the anatomical  
512 image and the mean functional image, and (4) spatial normalization of all images to a  
513 standard stereotaxic space (Montreal Neurological Institute, MNI) with a voxel size of 3x3x3  
514 mm<sup>3</sup>. Furthermore, the BOLD time series in MNI space were subjected to spatial

515 independent component analysis (ICA) for the identification and removal of artefacts related  
516 to blood pulsation, head movement and instrumental spikes (Smith et al., 2010). This BOLD  
517 artefact removal procedure was performed by means of the GIFT toolbox (Medical Image  
518 Analysis Lab, University of New Mexico). No global signal regression or spatial smoothing  
519 was applied to the preprocessed time series. For each recording (subject and run), we  
520 extracted the mean BOLD time series from the 66 regions of interest (ROIs) of the brain atlas  
521 (Hagmann et al., 2008)(**Supplementary Table 1**). We avoided regressing out nuisance  
522 parameters and using motion scrubbing, because the effects of these procedures on time-  
523 resolved FC analyses (phase locking values) could be unpredictable. 2 subjects were  
524 excluded due to signal dropout and 1 subject was excluded due to substantial spikes in the  
525 time-series.

526

### 527 **Anatomical Connectivity**

528

529 Anatomical connectivity was estimated from Diffusion Spectrum Imaging (DSI) data collected  
530 in five healthy right-handed male participants (Hagmann et al., 2008; Honey et al., 2009). The  
531 grey matter was first parcellated into 66 ROIs, using the same low-resolution atlas used for  
532 the FC analysis. For each subject, we performed white matter tractography between pairs of  
533 cortical areas to estimate a neuroanatomical connectivity matrix. The coupling weights  
534 between two brain areas were quantified using the fibre tract density, and were proportional  
535 to a normalized number of detected tracts. The structural matrix (SC) was then obtained by  
536 averaging the matrices over subjects.

537

### 538 **Principal component analysis**

539

540 For all subjects and runs (i.e. 21 subjects, 2 resting state and 2 movie runs) the functional  
541 connectivity matrices were constructed based on Pearson correlation coefficient between all  
542 pairs of ROIs.

543

544 The upper triangular parts of FC (i.e.  $66(66 - 1)/2$  connections) matrices were concatenated  
545 across subjects/runs (21x4 subjects/runs) leading to the feature matrix with dimensions 2145  
546 x 84 (number of connections x number of subjects/runs). Then, principal component analysis  
547 (PCA) was applied to the resulting feature matrix. To identify the noise components, the  
548 analyses were repeated for 1000 surrogate time-series for each subject/run. The properties of  
549 the surrogate time-series of each individual subject were preserved in spectral domain  
550 (Prichard and Theiler, 1994). The dimensionality of the data was characterized by the fraction  
551 of explained variance of the principal components that are larger than those of the surrogates.  
552 Since PCA decomposes the data into orthogonal axes with associated projections (i.e.  
553 scores) of each individual observation, we characterized the components based on these  
554 projections scores. The first PC might reflect the global synchronization levels. To quantify

555 this, we calculated the correlation between the first PC scores and the variance of global  
556 signal (i.e. the mean signal across regions). The principal component related to movie-  
557 watching condition was characterized as the one exhibiting clear separation between  
558 conditions based on the PC scores (i.e. the scores higher than 0 indicated the movie-  
559 watching runs, whereas the scores less than 0 indicated the resting-state runs).

560

561 To quantify the consistency of principal components, we repeated the analysis using 2  
562 separate runs. For both runs, the feature matrices comprised the concatenated upper  
563 triangular FC matrices of 1 resting state run and 1 movie run (i.e. 2145 x 42 matrices). The  
564 consistency was quantified as Pearson similarity of the components and their projections  
565 across runs (Supplementary Figure 1).

566

### 567 **Non-neuronal confounds**

568

569 During natural viewing condition the individuals are shown to have restricted movements and  
570 increase arousal (Vanderwal et al., 2015). Therefore, the differences in FC can be  
571 substantially affected by underlying artefacts. For each subject and run, we quantified head  
572 motion by calculating the mean frame-wise displacement (Power et al., 2012). **We checked**  
573 **for outliers with regards to head motion, and confirmed that no subject had a mean FD**  
574 **> 1mm.** We found no significant differences in mean frame-wise displacement across  
575 conditions ( $p=0.21$ , permutation  $t$ -test, 10000 permutations) (**mean FD resting state**  
576 **0.32±0.20; movie watching 0.35±0.23**). However, we observed condition-specific changes in  
577 motion parameters (i.e. several subjects consistently exhibited higher head movement during  
578 movie-runs, whereas other subjects exhibited lower head movement). To test this  
579 observation, we first used a regression model for mean frame-wise displacement:

580

581

$$y = \beta_0 + \beta_c X_c + \beta_t X_t + \beta_{int} X_c X_t$$

582

583 Where mean frame-wise displacement is  $y$ ,  $X_c$  is a dummy variable representing condition  
584 (resting-state vs. movie-watching),  $X_t$  is another variable representing each subject's  
585 tendency to exhibit increased/decreased movement during movie condition. The regression  
586 coefficient was not significant for the condition term ( $p=0.71$ ), but the coefficients were  
587 significant for tendency and the interaction terms ( $p=0.01$  and  $p=0.002$ , respectively). We also  
588 analysed the variations in mean frame-wise displacement using principal component analysis  
589 (PCA) over runs. We found that the second principal component (PC-2) explaining 16% of the  
590 variation was associated to the alterations in mean frame-wise displacement during movie-  
591 watching condition. The projections of PC-2, related to movie-watching mean frame-wise  
592 displacement, were not correlated with the projections of condition-specific PC (*Spearman*  
593 *rank*  $r=0.02$ ,  $p=0.85$ ).

594

595 Apart from head motion, various other confounding factors may affect during movie-watching  
596 condition. For this reason, we repeated all the analyses after regressing out the global signal  
597 from the time-series of each ROI for each subject and run.

598

#### 599 **Inter-subject synchronization**

600

601 To establish the construct validity of the principal component topography, we compared the  
602 condition-specific PC with inter-subject synchronization functional connectivity (ISS-FC)(Kim  
603 et al., 2017; Simony et al., 2016). ISS-FC was proposed as a measure to remove the effects  
604 of spontaneous activity and to define inter-regional correlations based on common stimuli  
605 across subjects. To calculate ISS-FC, we randomly split the subjects into 2 groups (50  
606 random groups) and calculated the average BOLD time-series of each region over subjects  
607 per group. Then, we calculated the correlations between the average BOLD time-series  
608 across pairs of regions. This procedure was repeated separately for 2 resting-state and 2  
609 movie-watching runs, and the average ISS-FC across movie-runs were reported in the main  
610 results. Since the sample size in this study is small, we replicated the analyses in the  
611 previous studies (Kim et al., 2017) and demonstrated the ISS-FC at resting-state and movie-  
612 watching conditions (Supplementary Figure 2).

613

#### 614 **Time-resolved functional connectivity**

615

616 To extract time-resolved functional connectivity (dynamic FC; dFC), we used phase locking  
617 values (PLVs) of BOLD time series in a narrow frequency band (Demirtaş et al., 2016;  
618 Glerean et al., 2012). This approach enables the characterization of connectivity patterns at  
619 each time point, and it does not require specification of a window and a step-size, as in  
620 sliding-window analysis. The preprocessed time series were band-pass filtered in *0.04-*  
621 *0.07Hz* range to reduce the effects of low-frequency drift and high-frequency noise (Glerean  
622 et al., 2012). The Hilbert transform was then used to quantify instantaneous phase. The  
623 Hilbert transform,  $S(t) = A\cos(\varphi(t))$  of the preprocessed BOLD time series decomposes the  
624 signal into to an analytical signal  $S(t)$  with an instantaneous phase  $\varphi(t)$  and amplitude  $A$ . For  
625 each time point  $t$ , the difference  $\Delta\varphi_{ij}(t)$  between the phases of the respective ROIs was  
626 calculated, where  $i$  and  $j$  are the indices of each ROI. The phase differences were adjusted  
627 between 0 and  $\pi$  such that:

628

$$629 \quad \Delta\varphi_{ij}(t) = \begin{cases} |\varphi_i(t) - \varphi_j(t)|, & \text{if } |\varphi_i(t) - \varphi_j(t)| \leq \pi \\ 2\pi - |\varphi_i(t) - \varphi_j(t)|, & \text{otherwise} \end{cases} \quad 1$$

630

631 Then, the phase-locking values (PLVs),  $PLV_{ij}(t)$  were constructed using the phase differences  
632 normalized between 0 and 1, thereby representing perfect anti-synchronization and perfect  
633 synchronization respectively, such that:  $PLV_{ij}(t) = 1 - \Delta\varphi_{ij}(t)/\pi$ .

634

### 635 **PCA trajectories of time-resolved FC**

636

637 The principal component analysis was repeated for grand average PLVs, to establish the link  
638 between Pearson correlation-derived FCs and PLVs. Since the PLVs were more sensitive to  
639 global synchronization levels, we subtracted the mean from each average PLV matrix before  
640 performing any analyses. After identifying the grand average condition-specific PLV  
641 component, we performed PCA on concatenated PLVs over time for each subject (i.e. 2  
642 resting-state and 2 movie-watching runs). The condition-specific temporal components were  
643 identified as the PC with the highest similarity to the grand average condition-specific PLV  
644 component. We then characterized the trajectories (i.e. PC scores over time) of the condition-  
645 specific temporal components of the subjects. Here, the term “trajectory” was preferred over  
646 “scores” to highlight the fact that the PCA was performed over time. We asked whether the  
647 PC showing highest similarity to the condition-specific component distinguishes between  
648 resting-state and movie-watching trajectories. We quantified the condition-specific distinction  
649 by calculating the average distance between the median trajectories of the resting-state and  
650 movie-watching conditions. The distances between median trajectories were defined as the  
651 squared difference between median PC scores of resting-state and movie-watching  
652 trajectories. For each subject, we assessed the significance of the distinction by comparing  
653 the condition-specific distance against the surrogates. The trajectories of each subject were

654 randomly shuffled and then assigned into two groups. The p-values were based on the  
655 distance between condition-specific trajectories, relative to the surrogate distances. Since the  
656 individual PC trajectories are time-dependent, we assessed the difference between conditions  
657 across subjects by calculating the median distances across conditions and runs. For each  
658 subject, the median trajectory distance between resting-state and movie-watching conditions  
659 was calculated. Then, the distances between 2 separate runs of resting-state and movie-  
660 watching conditions were calculated. Finally, we performed a permutation t-test to compare  
661 the average distance across conditions and runs.

662

### 663 **Time-resolved FC similarity across conditions and runs**

664

665 To study the role of time-locked events on PLV dynamics during movie-watching condition  
666 (analogous to inter-subject synchronization), we calculated the similarity between  
667 instantaneous PLVs across conditions and runs. For each time point, we calculated the  
668 similarity between the PLVs of a single subject (k) and the average PLVs across the rest of  
669 the subjects ( $n \neq k$ ). The average PLVs were calculated to test the PLV similarity in 3 different  
670 circumstances: Across conditions (i.e. if subject k is at resting state run 1, the average PLVs  
671 were calculated for movie-watching run 1), across runs (i.e. if subject k is at resting state run  
672 1, the average PLVs were calculated for resting state run 2) and within runs (i.e. if subject k is  
673 at resting state run 1, the average PLVs were calculated for resting state run 1).

674

### 675 **Computational modelling**

676

677 We modelled the whole-brain rs-fMRI BOLD signals using 66 nodes. Each node was coupled  
678 with each other via DWI-derived structural connectivity (SC) matrix. We described the local  
679 dynamics of each individual node using normal form of a supercritical Hopf bifurcation (Deco  
680 et al., 2017). The advantage of this model is that it allows transitions between asynchronous  
681 noise activity and oscillations. Where  $\omega$  is the intrinsic frequency of each node,  $a$  is the local  
682 bifurcation parameter,  $\eta$  is additive Gaussian noise with standard deviation  $\beta$ , the temporal  
683 evolution of the activity,  $z$ , in node  $j$  is given in complex domain as:

684

$$685 \quad \frac{dz_j}{dt} = [a_j + i\omega_j - |z_j|^2] + \beta\eta_j(t) \quad 2$$

686

687 and,

$$688 \quad z_j = \rho_j e^{i\theta_j} = x_j + iy_j \quad 3$$

689

690 This system shows a supercritical bifurcation at  $a_j = 0$ . Being specific, if  $a_j$  is smaller than 0,  
691 the local dynamics has a stable fixed point at  $z_j = 0$ , and for  $a_j$  values larger than 0, there

692 exists a stable limit cycle oscillation with a frequency  $f = \omega/2\pi$ . Finally, the whole-brain  
 693 dynamics is described by the following coupled equations:

694

$$695 \quad \frac{dx_j}{dt} = [a_j - x_j^2 - y_j^2]x_j - \omega_j y_j + g \sum_i C_{ij}(x_i - x_j) + \beta \eta_{xj}(t) \quad 4$$

696

$$697 \quad \frac{dy_j}{dt} = [a_j - x_j^2 - y_j^2]y_j + \omega_j x_j + g \sum_i C_{ij}(y_i - y_j) + \beta \eta_{yj}(t) \quad 5$$

698

699 Where  $C_{ij}$  is the Structural Connectivity (SC) between nodes  $i$  and  $j$ ,  $g$  is the global coupling  
 700 factor, and the standard deviation of Gaussian noise,  $\beta = 0.02$ . The natural frequency ( $f$ ) of  
 701 each region was taken as the peak frequency in the given narrowband of the corresponding  
 702 region in the empirical time-series.

703

704 Following a similar approach previously employed (Deco et al., 2014), we analytically  
 705 estimated the model FC using linearization of the system around a stable fix point. Where  
 706  $\delta \mathbf{u} = \{\delta x_1 \dots \delta x_{66}, \delta y_1 \dots \delta y_{66}\}$  represents the Taylor expansion of the system,  $\mathbf{A}$  is the  
 707 Jacobian matrix, and  $\varepsilon(t)$  is the noise term, the fluctuations around the fix point can be  
 708 described as:

$$709 \quad \frac{d\delta \mathbf{u}}{dt} = \mathbf{A}\delta \mathbf{u} + \varepsilon(t) \quad 6$$

710

711 Where the deterministic parts of right-hand side of equations 4 and 5 are described by  $-F_j$   
 712 and  $-G_j$ , respectively, the Jacobian matrix of the system evaluated at the fixed point  
 713  $\hat{x}_j, \hat{y}_j, j \in \{1 \dots 66\}$  can be constructed as:

714

$$715 \quad \mathbf{A} = \begin{bmatrix} \frac{\partial F_1}{\partial x_1} & \dots & \frac{\partial F_1}{\partial x_N} & \frac{\partial F_1}{\partial y_1} & \dots & \frac{\partial F_1}{\partial y_N} \\ \vdots & \ddots & \vdots & \vdots & \ddots & \vdots \\ \frac{\partial F_N}{\partial x_1} & \dots & \frac{\partial F_N}{\partial x_N} & \frac{\partial F_N}{\partial y_1} & \dots & \frac{\partial F_N}{\partial y_N} \\ \frac{\partial G_1}{\partial x_1} & \dots & \frac{\partial G_1}{\partial x_N} & \frac{\partial G_1}{\partial y_1} & \dots & \frac{\partial G_1}{\partial y_N} \\ \vdots & \ddots & \vdots & \vdots & \ddots & \vdots \\ \frac{\partial G_N}{\partial x_1} & \dots & \frac{\partial G_N}{\partial x_N} & \frac{\partial G_N}{\partial y_1} & \dots & \frac{\partial G_N}{\partial y_N} \end{bmatrix}$$

716

717 Where  $i, j \in \{1 \dots 66\}$ , each element of matrix  $\mathbf{A}$  can be calculated as:

718

$$719 \quad \frac{\partial F_j}{\partial x_j} = \frac{\partial G_j}{\partial y_j} = a - g \sum_k C_{jk} \quad 7$$

720

721 
$$\frac{\partial F_j}{\partial x_l} = \frac{\partial G_j}{\partial y_l} = gC_{jl} \quad 8$$

722

723 
$$\frac{\partial F_j}{\partial y_j} = -\omega_0 \quad 9$$

724

725 
$$\frac{\partial G_j}{\partial y_j} = \omega_0 \quad 10$$

726

727 
$$\frac{\partial F_j}{\partial x_l} = \frac{\partial G_j}{\partial y_l} = 0 \quad 11$$

728

729 Where  $\mathbf{Q}$  is the noise covariance matrix, the covariance matrix of the system  $\mathbf{P}$  can be  
 730 estimated by solving Lyapunov equation:

731

732 
$$\mathbf{AP} + \mathbf{PA}^T = -\mathbf{Q} \quad 12$$

733

734 Finally, the model correlation matrix (FC) can be extracted from the covariance matrix as:

735

736 
$$mFC_{ij} = \frac{P_{ij}}{\sqrt{P_{ii}P_{jj}}}, i, j \in \{1 \dots 66\} \quad 13$$

737

738 We estimated the model optimal parameters  $a$  and  $g$  by maximizing the similarity between  
 739 model FC (equation 13) and empirical FC using gradient descent optimization. For each  
 740 subject, the empirical functional connectivity was calculated as the average FC across the  
 741 corresponding conditions (i.e. resting state or movie sessions) of the corresponding subject.  
 742 The similarity between model FC and empirical FC was quantified as Pearson correlation  
 743 similarity. To avoid the solutions reflecting a local minimum, for each subject/condition we  
 744 estimated the best solution after repeating the optimization with 100 random initial conditions.

745

746

747 **Statistical analyses**

748

749 The comparisons across conditions (resting-state versus movie sessions) were done using  
 750 permutation t-test. Since the same subjects were tested under different conditions, we used  
 751 dependent t-test. The randomization during the permutation t-test was also controlled to  
 752 preserve this dependence across conditions. For optimal bifurcation parameters, the p-values  
 753 were FDR corrected ( $p < 0.01$ ), with the Benjamini & Hochberg algorithm, when appropriate  
 754 (Hochberg and Benjamini, 1990).

755

756 To assess the association between measures, we used Spearman rank correlations (to avoid  
757 potential contribution of outliers and due to limited sample size). Calculating the correlations  
758 separately for each condition (due to repeated-measures) did not alter the significance;  
759 therefore, for simplicity we reported a single correlation value between each measure. We  
760 used Pearson correlation as a measure of similarity between connectivity matrices (i.e. PC  
761 axes, FCs, PLVs).

762

763 The visualizations of the cortical surface were done using Connectome Workbench software.  
764 We used a population-average cortical surface (Conte69) (Van Essen, 2005), and a template  
765 to visualize the anatomical parcellations on the cortical surface.

766

- 768 Allen, E.A., Damaraju, E., Plis, S.M., Erhardt, E.B., Eichele, T., Calhoun, V.D., 2012. Tracking Whole-  
769 Brain Connectivity Dynamics in the Resting State. *Cereb. Cortex* bhs352.  
770 <https://doi.org/10.1093/cercor/bhs352>
- 771 Baars, B.J., 1993. A cognitive theory of consciousness., A cognitive theory of consciousness.  
772 Cambridge University Press, New York, NY, US.
- 773 Betti, V., Della Penna, S., de Pasquale, F., Mantini, D., Marzetti, L., Romani, G.L., Corbetta, M., 2013.  
774 Natural scenes viewing alters the dynamics of functional connectivity in the human brain.  
775 *Neuron* 79, 782–797. <https://doi.org/10.1016/j.neuron.2013.06.022>
- 776 Bijsterbosch, J., Harrison, S., Duff, E., Alfaro-Almagro, F., Woolrich, M., Smith, S., 2017. Investigations  
777 into within- and between-subject resting-state amplitude variations. *NeuroImage* 159, 57–69.  
778 <https://doi.org/10.1016/j.neuroimage.2017.07.014>
- 779 Biswal, B., Yetkin, F.Z., Haughton, V.M., Hyde, J.S., 1995. Functional connectivity in the motor cortex of  
780 resting human brain using echo-planar MRI. *Magn Reson Med* 34, 537–541.
- 781 Brookes, M.J., Woolrich, M., Luckhoo, H., Price, D., Hale, J.R., Stephenson, M.C., Barnes, G.R., Smith,  
782 S.M., Morris, P.G., 2011. Investigating the electrophysiological basis of resting state networks  
783 using magnetoencephalography. *PNAS* 108, 16783–16788.  
784 <https://doi.org/10.1073/pnas.1112685108>
- 785 Brovelli, A., Ding, M., Ledberg, A., Chen, Y., Nakamura, R., Bressler, S.L., 2004. Beta oscillations in a  
786 large-scale sensorimotor cortical network: Directional influences revealed by Granger causality.  
787 *Proceedings of the National Academy of Sciences* 101, 9849–9854.  
788 <https://doi.org/10.1073/pnas.0308538101>
- 789 Burt, J.B., Demirtas, M., Eckner, W.J., Navejar, N.M., Ji, J.L., Martin, W.J., Bernacchia, A., Anticevic, A.,  
790 Murray, J.D., in Press. Hierarchy of transcriptomic specialization across human cortex captured  
791 by myelin map topography. *Nat. Neurosci.*
- 792 Carbonell, F., Bellec, P., Shmuel, A., 2011. Global and System-Specific Resting-State fMRI Fluctuations  
793 Are Uncorrelated: Principal Component Analysis Reveals Anti-Correlated Networks. *Brain*  
794 *Connect* 1, 496–510. <https://doi.org/10.1089/brain.2011.0065>
- 795 Cole, M.W., Bassett, D.S., Power, J.D., Braver, T.S., Petersen, S.E., 2014. Intrinsic and Task-Evoked  
796 Network Architectures of the Human Brain. *Neuron* 83, 238–251.  
797 <https://doi.org/10.1016/j.neuron.2014.05.014>
- 798 Cole, M.W., Ito, T., Bassett, D.S., Schultz, D.H., 2016. Activity flow over resting-state networks shapes  
799 cognitive task activations. *Nat Neurosci* 19, 1718–1726. <https://doi.org/10.1038/nn.4406>
- 800 Craddock, R.C., Holtzheimer, P.E., Hu, X.P., Mayberg, H.S., 2009. Disease state prediction from resting  
801 state functional connectivity. *Magn. Reson. Med.* 62, 1619–1628.  
802 <https://doi.org/10.1002/mrm.22159>
- 803 Deco, G., Kringelbach, M.L., Jirsa, V.K., Ritter, P., 2017. The dynamics of resting fluctuations in the  
804 brain: metastability and its dynamical cortical core. *Scientific Reports* 7.  
805 <https://doi.org/10.1038/s41598-017-03073-5>
- 806 Deco, G., Ponce-Alvarez, A., Hagmann, P., Romani, G.L., Mantini, D., Corbetta, M., 2014. How Local  
807 Excitation-Inhibition Ratio Impacts the Whole Brain Dynamics. *The Journal of Neuroscience*  
808 34, 7886–7898. <https://doi.org/10.1523/JNEUROSCI.5068-13.2014>
- 809 Deco, G., Tononi, G., Boly, M., Kringelbach, M.L., 2015. Rethinking segregation and integration:  
810 contributions of whole-brain modelling. *Nature Reviews Neuroscience* 16, 430–439.  
811 <https://doi.org/10.1038/nrn3963>
- 812 Demirtaş, M., Tornador, C., Falcón, C., López-Solà, M., Hernández-Ribas, R., Pujol, J., Menchón, J.M.,  
813 Ritter, P., Cardoner, N., Soriano-Mas, C., Deco, G., 2016. Dynamic functional connectivity  
814 reveals altered variability in functional connectivity among patients with major depressive  
815 disorder. *Hum. Brain Mapp.* 37, 2918–2930. <https://doi.org/10.1002/hbm.23215>
- 816 Finn, E.S., Shen, X., Scheinost, D., Rosenberg, M.D., Huang, J., Chun, M.M., Papademetris, X.,  
817 Constable, T.R., 2015. Functional connectome fingerprinting: identifying individuals using  
818 patterns of brain connectivity 18, 1664–1671. <https://doi.org/10.1038/nn.4135>
- 819 Friston, K., 2010. The free-energy principle: a unified brain theory? *Nature Reviews Neuroscience* 11,  
820 127–138. <https://doi.org/10.1038/nrn2787>
- 821 Gilson, M., Deco, G., Friston, K.J., Hagmann, P., Mantini, D., Betti, V., Romani, G.L., Corbetta, M.,  
822 2017. Effective connectivity inferred from fMRI transition dynamics during movie viewing points  
823 to a balanced reconfiguration of cortical interactions. *NeuroImage*.  
824 <https://doi.org/10.1016/j.neuroimage.2017.09.061>
- 825 Glerean, E., Salmi, J., Lahnakoski, J.M., Jaaskelainen, I.P., Sams, M., 2012. Functional Magnetic  
826 Resonance Imaging Phase Synchronization as a Measure of Dynamic Functional Connectivity.  
827 *Brain Connect* 2, 91–101. <https://doi.org/10.1089/brain.2011.0068>
- 828 Gonzalez-Castillo, J., Hoy, C.W., Handwerker, D.A., Robinson, M.E., Buchanan, L.C., Saad, Z.S.,  
829 Bandettini, P.A., 2015. Tracking ongoing cognition in individuals using brief, whole-brain  
830 functional connectivity patterns. *Proceedings of the National Academy of Sciences* 112, 8762–  
831 8767. <https://doi.org/10.1073/pnas.1501242112>
- 832 Gross, J., Schmitz, F., Schnitzler, I., Kessler, K., Shapiro, K., Hommel, B., Schnitzler, A., 2004.  
833 Modulation of long-range neural synchrony reflects temporal limitations of visual attention in

834 humans. *Proceedings of the National Academy of Sciences* 101, 13050–13055.  
835 <https://doi.org/10.1073/pnas.0404944101>

836 Hagmann, P., Cammoun, L., Gigandet, X., Meuli, R., Honey, C.J., Wedeen, V.J., Sporns, O., 2008.  
837 Mapping the Structural Core of Human Cerebral Cortex. *PLoS Biol* 6, e159.  
838 <https://doi.org/10.1371/journal.pbio.0060159>

839 Hasson, U., 2004. Intersubject Synchronization of Cortical Activity During Natural Vision. *Science* 303,  
840 1634–1640. <https://doi.org/10.1126/science.1089506>

841 Hasson, U., Malach, R., Heeger, D.J., 2010. Reliability of cortical activity during natural stimulation.  
842 *Trends in Cognitive Sciences* 14, 40–48. <https://doi.org/10.1016/j.tics.2009.10.011>

843 Hipp, J.F., Havelle, D.J., Corbetta, M., Siegel, M., Engel, A.K., 2012. Large-scale cortical correlation  
844 structure of spontaneous oscillatory activity. *Nature Neuroscience* 15, 884–890.  
845 <https://doi.org/10.1038/nn.3101>

846 Hochberg, Y., Benjamini, Y., 1990. More powerful procedures for multiple significance testing. *Statist.*  
847 *Med.* 9, 811–818. <https://doi.org/10.1002/sim.4780090710>

848 Honey, C.J., Sporns, O., Cammoun, L., Gigandet, X., Thiran, J.P., Meuli, R., Hagmann, P., 2009.  
849 Predicting human resting-state functional connectivity from structural connectivity. *PNAS* 106,  
850 2035–2040. <https://doi.org/10.1073/pnas.0811168106>

851 Kim, D., Kay, K., Shulman, G.L., Corbetta, M., 2017. A New Modular Brain Organization of the BOLD  
852 Signal during Natural Vision. *Cerebral Cortex* 1–17. <https://doi.org/10.1093/cercor/bhx175>

853 Mantini, D., Corbetta, M., Romani, G.L., Orban, G.A., Vanduffel, W., 2012. Data-driven analysis of  
854 analogous brain networks in monkeys and humans during natural vision. *NeuroImage* 63,  
855 1107–1118. <https://doi.org/10.1016/j.neuroimage.2012.08.042>

856 Power, J.D., Barnes, K.A., Snyder, A.Z., Schlaggar, B.L., Petersen, S.E., 2012. Spurious but systematic  
857 correlations in functional connectivity MRI networks arise from subject motion. *NeuroImage* 59,  
858 2142–2154. <https://doi.org/10.1016/j.neuroimage.2011.10.018>

859 Power, J.D., Plitt, M., Laumann, T.O., Martin, A., 2017. Sources and implications of whole-brain fMRI  
860 signals in humans. *NeuroImage* 146, 609–625.  
861 <https://doi.org/10.1016/j.neuroimage.2016.09.038>

862 Prichard, D., Theiler, J., 1994. Generating Surrogate Data for Time Series with Several Simultaneously  
863 Measures Variables. *Physical Review Letters* 73, 951–954.

864 Rosenberg, M.D., Finn, E.S., Scheinost, D., Papademetris, X., Shen, X., Constable, R.T., Chun, M.M.,  
865 2015. A neuromarker of sustained attention from whole-brain functional connectivity. *Nature*  
866 *Neuroscience* 19, 165–171. <https://doi.org/10.1038/nn.4179>

867 Shine, J.M., Breakspear, M., Bell, P., Ehgoetz Martens, K., Shine, R., Koyejo, O., Sporns, O., Poldrack,  
868 R., 2018. The dynamic basis of cognition: an integrative core under the control of the  
869 ascending neuromodulatory system. <https://doi.org/10.1101/266635>

870 Siegel, J.S., Mitra, A., Laumann, T.O., Seitzman, B.A., Raichle, M., Corbetta, M., Snyder, A.Z., 2016.  
871 Data Quality Influences Observed Links Between Functional Connectivity and Behavior.  
872 *Cerebral Cortex*. <https://doi.org/10.1093/cercor/bhw253>

873 Siegel, M., Donner, T.H., Oostenveld, R., Fries, P., Engel, A.K., 2008. Neuronal Synchronization along  
874 the Dorsal Visual Pathway Reflects the Focus of Spatial Attention. *Neuron* 60, 709–719.  
875 <https://doi.org/10.1016/j.neuron.2008.09.010>

876 Simony, E., Honey, C.J., Chen, J., Lositsky, O., Yeshurun, Y., Wiesel, A., Hasson, U., 2016. Dynamic  
877 reconfiguration of the default mode network during narrative comprehension. *Nature*  
878 *Communications* 7, 12141. <https://doi.org/10.1038/ncomms12141>

879 Smith, J.F., Pillai, A., Chen, K., Horwitz, B., 2010. Identification and validation of effective connectivity  
880 networks in functional magnetic resonance imaging using switching linear dynamic systems.  
881 *NeuroImage* 52, 1027–1040. <https://doi.org/10.1016/j.neuroimage.2009.11.081>

882 Smith, S., 2016. Linking cognition to brain connectivity. *Nat Neurosci* 19, 7–9.  
883 <https://doi.org/10.1038/nn.4206>

884 Stephan, K.E., Diaconescu, A.O., Iglesias, S., 2016. Bayesian inference, dysconnectivity and  
885 neuromodulation in schizophrenia. *Brain* 139, 1874–1876.  
886 <https://doi.org/10.1093/brain/aww120>

887 Tavor, I., Jones, O.P., Mars, R.B., Smith, S.M., Behrens, T.E., Jbabdi, S., 2016. Task-free MRI predicts  
888 individual differences in brain activity during task performance. *Science* 352, 216–220.  
889 <https://doi.org/10.1126/science.aad8127>

890 Tononi, G., 2004. An information integration theory of consciousness. *BMC Neuroscience* 5, 42.  
891 <https://doi.org/10.1186/1471-2202-5-42>

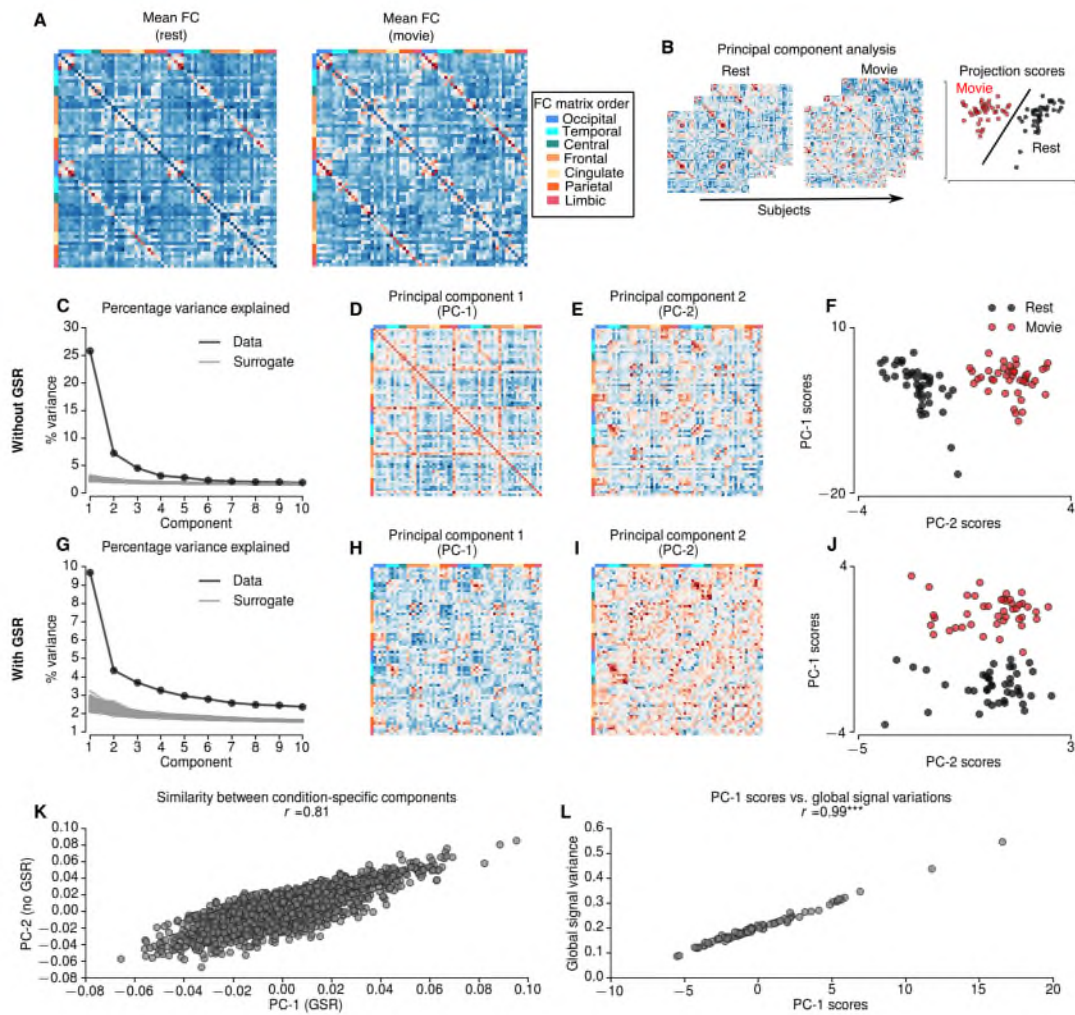
892 Utevsky, A.V., Smith, D.V., Huettel, S.A., 2014. Precuneus Is a Functional Core of the Default-Mode  
893 Network. *J Neurosci* 34, 932–940. <https://doi.org/10.1523/JNEUROSCI.4227-13.2014>

894 Van Essen, D.C., 2005. A Population-Average, Landmark- and Surface-based (PALS) atlas of human  
895 cerebral cortex. *NeuroImage* 28, 635–662. <https://doi.org/10.1016/j.neuroimage.2005.06.058>

896 Vanderwal, T., Eilbott, J., Finn, E.S., Craddock, R.C., Turnbull, A., Castellanos, F.X., 2017. Individual  
897 differences in functional connectivity during naturalistic viewing conditions. *NeuroImage* 157,  
898 521–530. <https://doi.org/10.1016/j.neuroimage.2017.06.027>

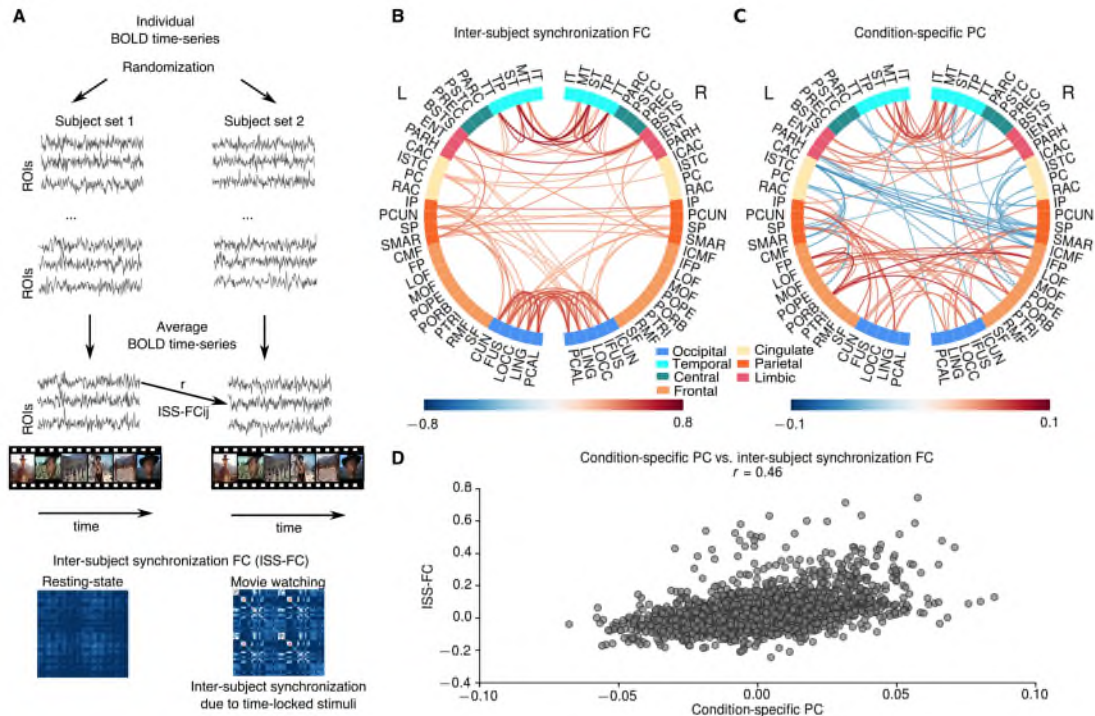
899 Vanderwal, T., Kelly, C., Eilbott, J., Mayes, L.C., Castellanos, F.X., 2015. Inscapes : A movie paradigm  
900 to improve compliance in functional magnetic resonance imaging. *NeuroImage* 122, 222–232.

901 <https://doi.org/10.1016/j.neuroimage.2015.07.069>  
902 Wolf, I., Dziobek, I., Heekeren, H.R., 2010. Neural correlates of social cognition in naturalistic settings: A  
903 model-free analysis approach. *NeuroImage* 49, 894–904.  
904 <https://doi.org/10.1016/j.neuroimage.2009.08.060>  
905 Zhou, Y., Friston, K.J., Zeidman, P., Chen, J., Li, S., Razi, A., 2018. The Hierarchical Organization of  
906 the Default, Dorsal Attention and Salience Networks in Adolescents and Young Adults.  
907 *Cerebral Cortex* 28, 726–737. <https://doi.org/10.1093/cercor/bhx307>  
908  
909



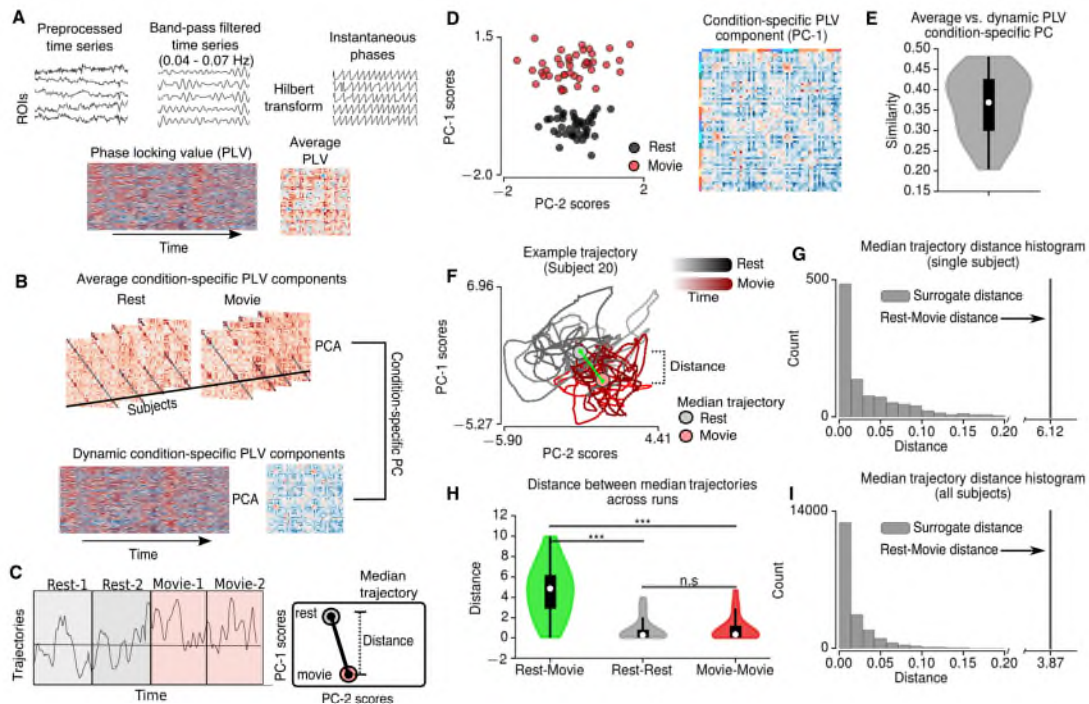
911  
 912  
 913  
 914  
 915  
 916  
 917  
 918  
 919  
 920  
 921

**Figure 1.** **A** Mean functional connectivity (FC) during resting-state and movie-watching conditions. **B** Schematic describing principal component analysis (PCA) over FCs of 2 resting-state and 2 movie-watching condition concatenated across 21 subjects. **C-F** PCA results without global signal regression (GSR). Explained variance by each PC (black) and random surrogates (gray) without GSR (**C**). Compared to 1000 random surrogates the dimensionality of FCs without GSR was 13. The first PC (**D**) explains 25.8% of the variation, whereas second PC (**E**) explains 7.2% of the variation. The projections of first two PCs shows that the second component is specific to movie runs (**F**). The first PC of the FCs without GSR reflects global signal standard deviation (**L**). **G-J** PCA results with global signal regression (GSR). **G** Explained variance by each PC (black) and random surrogates (gray) with GSR. Compared to random surrogates the dimensionality of FCs with GSR is 22. The first PC, which is specific to movie runs explains 9.69% of the variation (**J**). **K** The similarity between condition-specific components with and without GSR. \*\*\* indicates  $p < 0.0001$ .



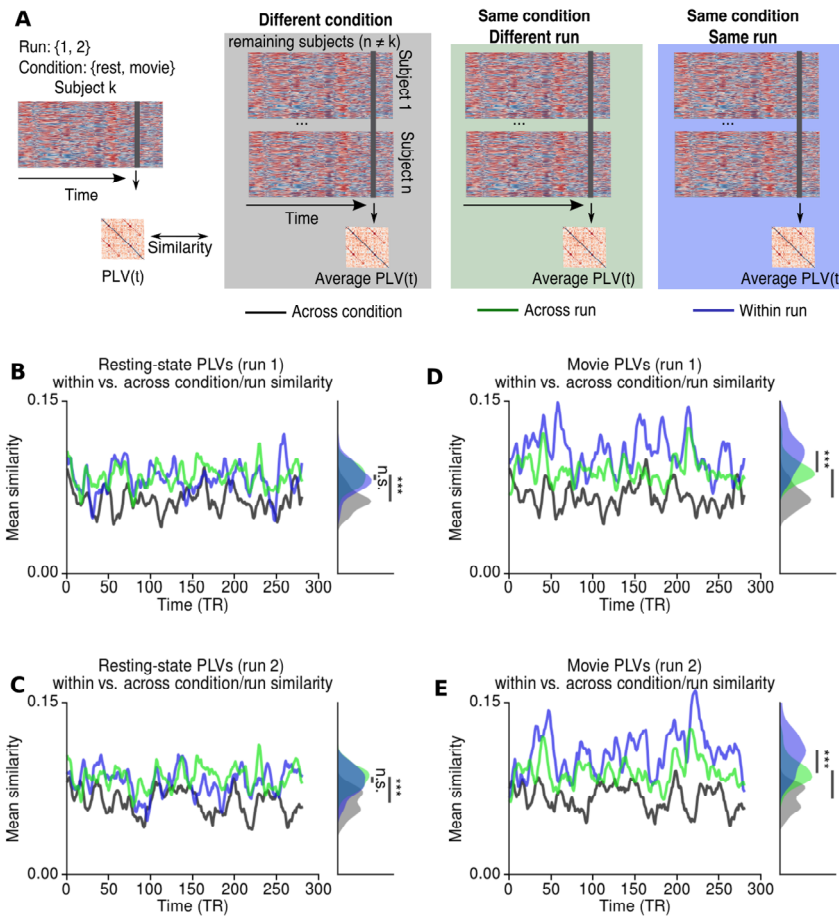
922  
 923  
 924  
 925  
 926  
 927  
 928  
 929  
 930  
 931

**Figure 2.** Comparison of condition-specific PC and inter-subject synchronization FC. **A** Schematic illustrating the computation of inter-subject synchronization FC (ISS-FC). The subjects were randomly separated into 2 groups. Then the average BOLD time-series were calculated for each group. ISS-FCs were computed as the correlation between BOLD time-series across groups for each pair of regions. **B** The largest 100 connections in ISS-FC during movie-watching condition. The most prominent correlations were observed among occipital and temporal brain regions, and between occipital and parietal brain regions. **C** The largest 100 connections in condition-specific PC. Condition-specific PC also shows increased connectivity among occipital and temporal brain regions, and between occipital and parietal brain regions; and the overall connectivity pattern in ISS-FC and condition-specific PC was highly similar (**D**). However, the condition-specific PC also exhibited increased connectivity among frontal brain regions and suppressed connectivity between cingulate and parietal regions (**C**).



932  
 933  
 934  
 935  
 936  
 937  
 938  
 939  
 940  
 941  
 942  
 943  
 944

**Figure 3.** Time-resolved FC based on phase locking values (PLVs). **A** Schematic describing the calculation of PLVs. Preprocessed BOLD time-series were narrow-band filtered in 0.04-0.07Hz range and the resulting signals were Hilbert transformed. Phase-locking values were calculated based on the difference between instantaneous phases across brain regions. **B** Schematic describing principal component analysis (PCA) performed on average PLVs across subjects (top) and dynamics of PLVs across time for each subject (bottom). A condition-specific component was identified based on the maximum similarity between dynamic PLV components and average condition-specific PLV component (**D**). The average and dynamic condition-specific components were very similar across subjects (**E**). Based on the trajectories of condition-specific PLV components, the distance between the median trajectories of resting-state and movie-watching conditions were calculated (**C**). **F** Example trajectory for single subject. **G** The distance between the median trajectories of resting-state and movie-watching conditions compared to the histogram of the distances for 1000 randomly split trajectories. **H** The median trajectory distances between resting-state and movie-watching conditions, between 2 resting-state runs and between 2 movie-watching runs. The distance between conditions was significantly higher than the distance between runs (permutation t-test, 10000 permutations). \*\*\* indicates  $p < 0.0001$ , n.s. indicates  $p > 0.05$ .



945  
 946  
 947  
 948  
 949  
 950  
 951  
 952  
 953  
 954  
 955  
 956

**Figure 4.** Time-resolved similarity between PLVs across conditions and runs. **A** Schematic describing the procedure. For each subject the PLVs at each time point was compared to the average PLVs across the remaining subjects at the same time point. Black/gray lines/shades indicate that the average PLVs were calculated for different condition (i.e. if subject k is at rest, average PLVs were calculated for movie-watching). Green lines/shades indicate that the PLVs were calculated for the same condition but different run (i.e. if subject k is at rest in run 1, average PLVs were calculated for the resting-state run 2). Blue lines/shades indicate that the PLVs were calculated for the same condition and the same run (i.e. if subject k is at rest in run 1, average PLVs were calculated for the resting-state run 1). **B-C** During resting-state the similarity between PLVs were significantly lower across conditions (i.e. rest vs. movie), but there was no significant difference between the similarities across runs. **D-E** During movie-watching, the similarity between PLVs was significantly lower across conditions. However, the similarity between PLVs was significantly higher within runs compared to across runs. The histograms illustrates the distributions of similarity measures over time, whereas \*\*\* indicates the  $p < 0.0001$  assessed by permutation t-test across subjects. n.s. indicates  $p > 0.05$ .

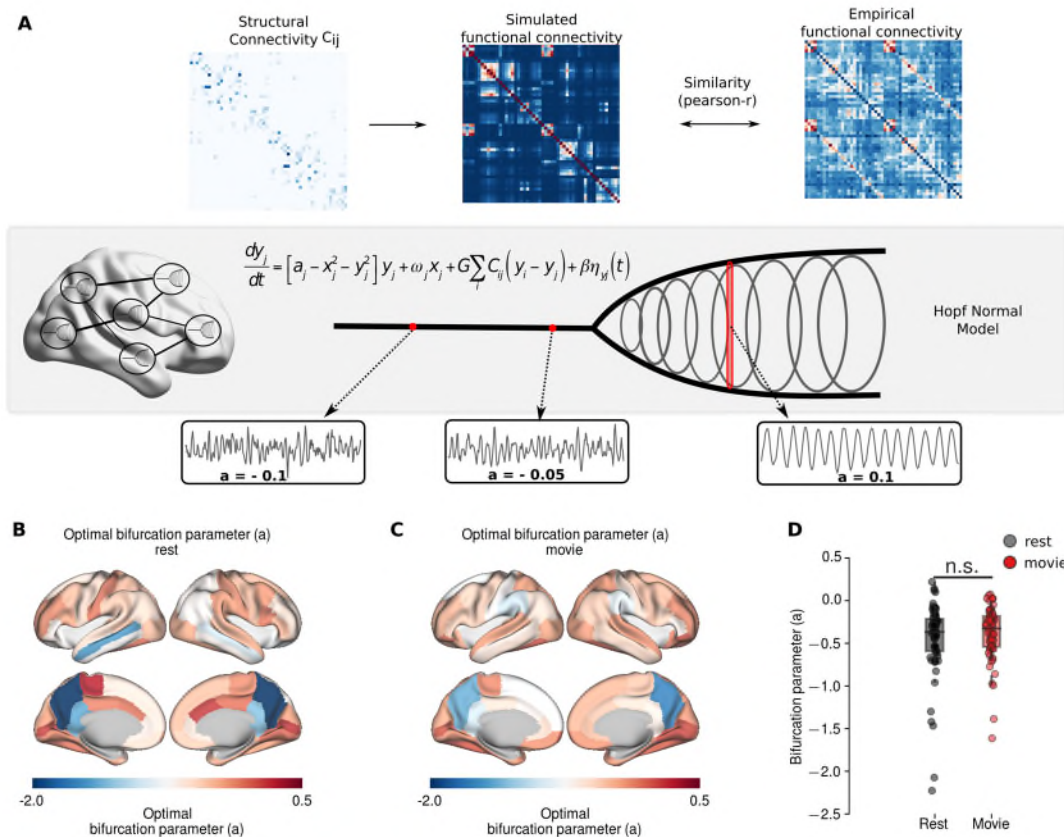


**Figure 5.** Large-scale computational modelling. **A** The schematic of the modelling framework. The BOLD activity of each region was described using Hopf normal model, where the local bifurcation parameters ( $a$ ) mediate the local dynamics. Negative values of bifurcation parameter,  $a$ , indicates noise-driven activity, whereas positive values indicate oscillatory activity with increasing amplitude. Brain regions are coupled each other through DWI-derived SC matrix. The optimal model parameters were estimated using gradient descent optimization, which maximizes the similarity between empirical and model FC. **B** Mean optimal bifurcation parameter topography at resting state. **C** Mean optimal bifurcation parameter topography during movie condition. **D** The distributions of the bifurcation parameters during movie condition and resting state. n.s. indicate  $p > 0.05$ .

957  
958  
959  
960  
961  
962  
963  
964  
965

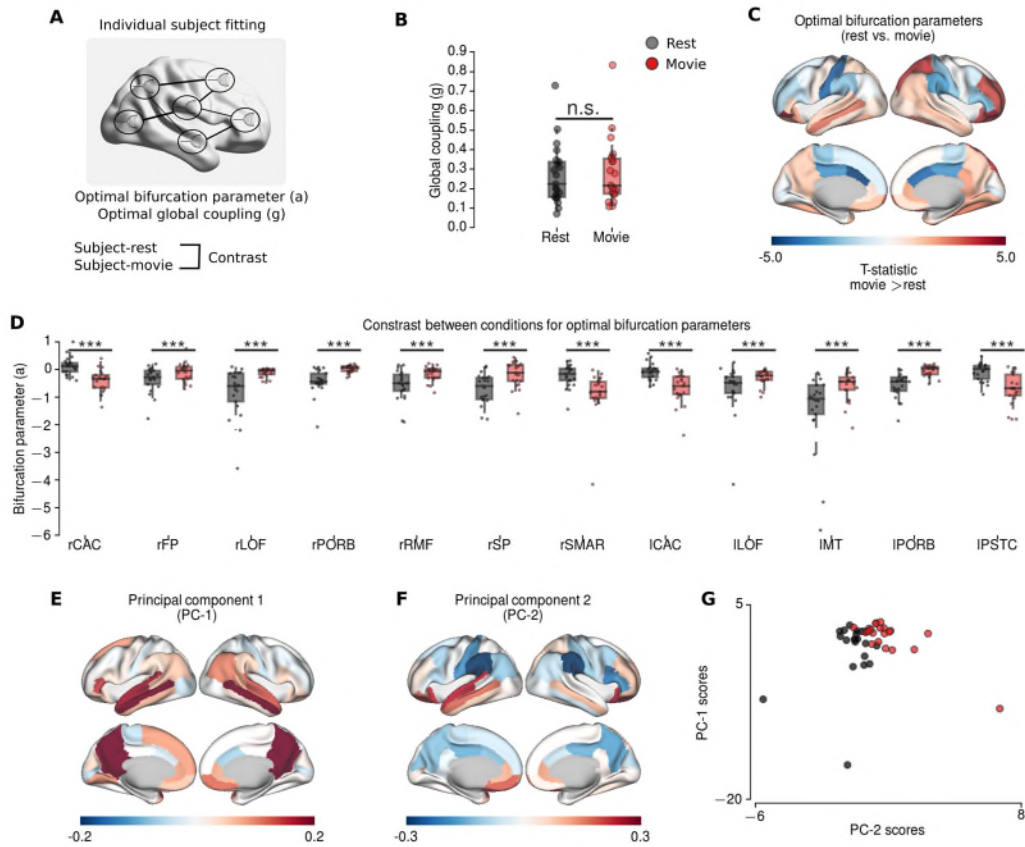


**Figure 6.** Modelling results for individual subject fitting. **A** The schematic of individual subject fitting. **B** The group differences for global coupling parameters did not show significant difference. **C-D** The group differences between optimal bifurcation parameters at rest (black) and during movie condition (red) (permutation t-test, 10000 permutations). **C** The topography of the group differences (T-statistics; hot colours indicate larger values during movie condition). **D** Boxplots of the regions showing significantly difference after FDR correction ( $p < 0.01$ ). **E-G** Principal component analysis applied to optimal bifurcation parameters in the model. **E** The topography of the first principal component. **F** The topography of the second principal component. PC-1 has higher values in precuneus, posterior cingulate, medial temporal and frontal regions, exhibiting typical pattern associated to default mode network. PC-2 exhibit increased values in frontal and temporal regions, and decreased values particularly in supramarginal gyrus consistent with the contrast between conditions. **G** The projections of the principal components on rest and movie conditions. \*\*\* indicates  $p < 0.01$ , n.s. indicates  $p > 0.05$ .

966  
 967  
 968  
 969  
 970  
 971  
 972  
 973  
 974  
 975  
 976